

1 **Improving Runoff Simulation in the Western United States with**
2 **Noah-MP and VIC**

3 Lu Su^{a,b}, Dennis P. Lettenmaier^b, Ming Pan^a, Benjamin Bass^c

4 a Center for Western Weather and Water Extremes, Scripps Institution of Oceanography,
5 University of California, San Diego, United States

6 b Department of Geography, University of California, Los Angeles, United States

7 c Department of Atmospheric and Oceanic Sciences, University of California, Los Angeles,
8 United States

9 Correspondence: Dennis P. Lettenmaier (dlettenm@ucla.edu)

10 **Abstract**

11 Streamflow predictions are critical for managing water resources and for
12 environmental conservation, especially in the water-short Western U.S. Land Surface
13 Models (LSMs), such as the Variable Infiltration Capacity (VIC) model and the Noah-
14 Multiparameterization (Noah-MP) play an essential role in providing comprehensive
15 runoff predictions across the region. Virtually all LSMs require parameter estimation
16 (calibration) to optimize their predictive capabilities. Here, we focus on the
17 calibration of VIC and Noah-MP models at a 1/16° latitude-longitude resolution
18 across the Western U.S. We first performed global optimal calibration of parameters
19 for both models for 263 river basins in the region. We find that the calibration
20 significantly improves the models' performance, with the median daily streamflow
21 Kling-Gupta Efficiency (KGE) increasing from 0.37 to 0.70 for VIC, and from 0.22 to
22 0.54 for Noah-MP. In general, post-calibration model performance is higher for
23 watersheds with relatively high precipitation and runoff ratios, and at lower elevations.
24 At a second stage, we regionalize the river basin calibrations using the donor-basin
25 method, which establishes transfer relationships for hydrologically similar basins, via

26 which we extend our calibration parameters to 4,816 HUC-10 basins across the region.
27 Using the regionalized parameters, we show that the models' capabilities to simulate
28 high and low flow conditions are substantially improved following calibration and
29 regionalization. The refined parameter sets we developed are intended to support
30 regional hydrological studies and hydrological assessments of climate change impacts.

31

32 **1. Introduction**

33 Streamflow predictions play a key role in water and environmental management,
34 especially in the water-stressed Western U.S. (WUS). In the short term, these
35 predictions provide early warnings for impending flood events, thereby enabling
36 timely preparation and response to mitigate immediate flood risk and damages (Raff
37 et al., 2013; Maidment, 2017). (In the longer term, streamflow predictions enable
38 water utilities and agencies to plan water distribution within and across multiple
39 uses—urban, agricultural, and industrial (Anghileri et al., 2016). Streamflow
40 predictions also aid in understanding and foreseeing the impacts of climate change on
41 water systems, thereby informing adaptive strategies for water resource management.

42 Streamflow predictions are derived via a synthesis of hydrometeorological data,
43 statistical methodologies, and computational modeling. Direct measurement of runoff
44 is an important element of this process, however it is only possible in river basins with
45 well-developed observational infrastructure (Sharma and Machiwal, 2021). This
46 limitation leaves vast areas, often critical to water resource management and
47 climatology, without direct runoff observations on which to base streamflow
48 predictions. As an alternative, Land Surface Models (LSMs) can be used to simulate
49 streamflow. LSMs typically are forced with air temperature, precipitation and other
50 surface meteorological variables. By integrating climatic, topographic, and land-use
51 information, they can fill streamflow observation gaps and provide comprehensive,

52 spatially distributed runoff predictions (Fisher and Koven, 2020). The capabilities of
53 LSMs equip us with the necessary tools to produce streamflow predictions that can be
54 used to prepare for severe weather conditions, form the basis for water resource
55 management, and inform water management associated with our evolving climate.

56 One of the key challenges in hydrological modeling is the reliable representation
57 of the spatiotemporal variability of natural processes (Dembélé et al., 2020).
58 Enhanced spatial resolution and improved estimates of surface meteorological
59 variables have empowered LSMs to predict diverse processes with greater detail.
60 However, a recurrent issue is that the parameters embedded in LSMs often
61 inadequately capture fine-scale variations in land surface processes, as illustrated in
62 Figures S7 and S8. Accurate prediction of land surface processes, particularly over
63 large areas, requires accurate parameter estimation, which remains a significant
64 bottleneck. Errors in parameter estimates affect LSMs' ability to forecast runoff at
65 continental or subcontinental scales. Fisher and Koven (2020) identify LSM
66 parameter estimation as one of three grand challenges in land surface modeling.

67 To deal with this challenge, we describe methods and resulting high-resolution
68 parameter data sets for two widely used LSMs across the WUS. We base our
69 estimates on a strategy of minimizing metrics of differences in observed and model-
70 predicted streamflow, following many previous studies (Arsenault and Brissette,
71 2014; Poissant et al., 2017; Razavi and Coulibaly, 2017; Gochis et al., 2019; Qi et al.,
72 2021 and Bass et al., 2023) We do so because streamflow observations are more
73 readily available than other model prognostic variables like soil moisture or
74 evapotranspiration (Demaria et al., 2007; Gao et al., 2018; Troy et al., 2008; Yadav et
75 al., 2007), although the methods we use could be generalized to incorporate other
76 observed and model-predicted fluxes and state variables. Although previous studies
77 have mostly focused on a single hydrologic model (e.g., Mascaro et al. (2023),

78 Sofokleous et al. (2023), and Gou et al. (2020)), here we utilize two models to address
79 structural model uncertainty and to ensure broader applicability of the calibration
80 methods we employ.

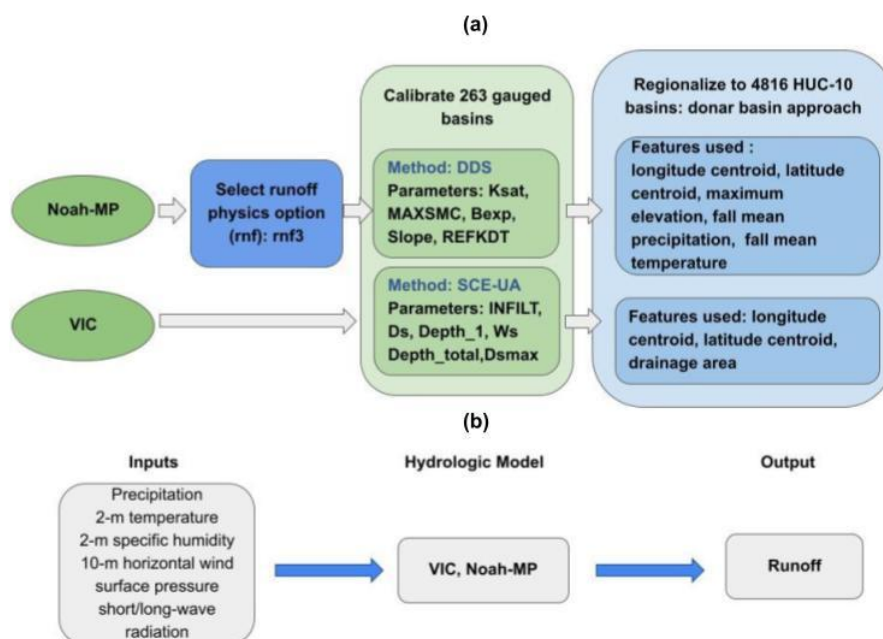
81 The Variable Infiltration Capacity (VIC, Liang et al. (1994)) model and Noah-
82 Multiparameterization (Noah-MP, Niu et al. (2011)), which we use here, are widely
83 used hydrologic models both in the U.S. and globally, as highlighted by Mendoza et al.
84 (2015) and Tangdamrongsub (2023). Many previous implementations of VIC for the
85 Western United States (WUS) have been based on the Livneh et al. (2013) data set,
86 and its predecessor, Maurer et al. (2002), which performed initial calibrations across
87 the region. In the case of Noah-MP, Bass et al. (2023) performed manual calibration
88 across the region. Neither of these implementations, however, employs globally
89 optimized calibration, as we do here.

90 The process of calibration can be computationally demanding, and prior research
91 typically has focused on obtaining parameters appropriate to facilitating model
92 simulations that match observations as closely as possible at stream gauge locations
93 (Duan et al,1992; Tolson and Shoemaker, 2007). Most previous studies have
94 concentrated on a limited number of gauges/river basins (e.g. Mascaro et al. (2023);
95 Sofokleous et al. (2023); and Gou et al. (2020)). Here, we aim to establish
96 parameterizations for VIC and Noah-MP across the entire WUS. In doing so, we
97 apply global optimization methods at 263 river basins, followed by a second stage
98 regionalization to the whole of WUS.

99 Specifically, the work we report here aims to develop calibration parameters for
100 the VIC and Noah-MP models that can be implemented at the catchment (Hydrologic
101 Unit Code or HUC) 10 level across the region. We explore and elucidate (i) the choice
102 of physical parameterizations and calibration of land surface parameters, (ii)
103 extension of these calibrated parameters to areas without gauges, and (iii) factors that

104 influence calibration efficiency and LSM performance using regional parameter
 105 estimates. Following this introduction, Section 2 describes our calibration basins, the
 106 hydrologic models used, and the forcing dataset. The framework of our procedures is
 107 illustrated in Figure 1. Section 3 provides an in-depth exploration of the calibration
 108 process. In the case of Noah-MP, which offers multiple runoff generation (physics)
 109 options, our initial step involves choosing the most effective runoff parameterization
 110 option. Following this, we perform the calibration of land surface parameters. In the
 111 case of the VIC model, the runoff parameterization scheme is predetermined, so we
 112 commence immediately with calibration at 263 river basins across our region. Our
 113 second stage regionalization (section 4) extends the calibrated parameters to ungauged
 114 basins using the technique known as the donor basin method, as implemented by Bass
 115 et al. (2023). In Section 5, we evaluate both flood and low flow simulation skills both
 116 pre- and post-calibration, and following regionalization. Finally, following discussion
 117 and interpretation (section 6) section 7 presents conclusions, encapsulating the
 118 insights and implications of our study.

119



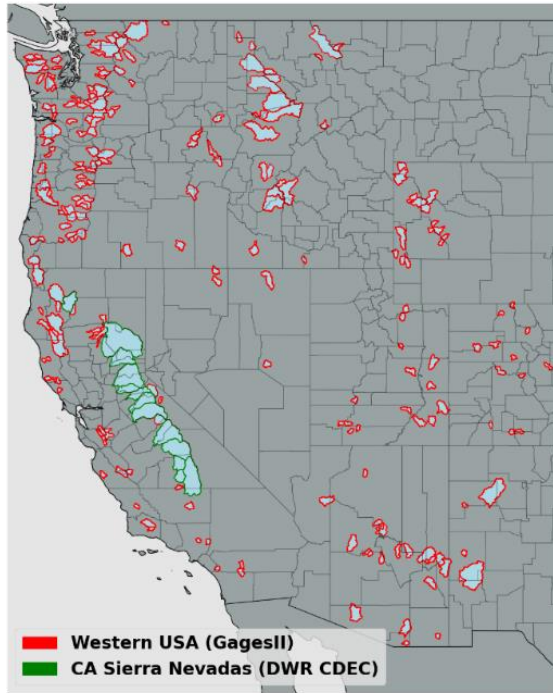
120

121 Figure 1 (a) framework of the calibration and regionalization processes adopted
122 in this study. (b) model simulation inputs and output.

123 **2. Study basins, land surface models and forcing dataset overview**

124 **2.1 Study Basins**

125 We selected 263 river basins distributed across the WUS for calibration of the
126 two models. Most of the basins were from USGS Gages II reference basins (Falcone
127 2011) which have minimum upstream anthropogenic effects such as dams and
128 diversions. Among these basins, our selection criteria included having at least 20
129 years of record, and a minimum drainage area of 144 square kilometers, which is the
130 size of four model grid cells. In addition to 250 Gages II reference stations, we
131 included 13 basins located in California's Sierra Nevada for which naturalized flows
132 (effects of upstream reservoir storage and/or diversions removed) are available from
133 the California Department of Water Resources (2021). The locations of the 263 basins
134 are shown in Figure 2. We used the most recent 20-year period of streamflow
135 observations for calibration in each of the 263 basins.



136

137 Figure. 2. 263 river basins for which calibration was performed. The Gages II
 138 reference basins are delineated with red boundaries and the CA Sierra Nevada basins
 139 with green boundaries.

140 **2.2 Land Surface Models**

141 The two models we used (VIC and Noah-MP) were chosen due to their broad
 142 application and proven effectiveness in hydrological simulations. The VIC model is
 143 renowned globally for its success in runoff simulation, as evidenced by studies such
 144 as Adam et al. (2003 & 2006), Livneh et al. (2013), and Schaperow et al. (2021).
 145 Conversely, Noah-MP, though relatively newer, forms the hydrologic core of the U.S.
 146 National Water Model (NWM) and is increasingly used both within the U.S. and
 147 abroad.

148 Our selection is further reinforced by a study conducted by Cai et al. (2014),
 149 which assessed the hydrologic performance of four LSMs in the United States using
 150 the North American Land Data Assimilation System (NLDAS) test bed. This study

151 highlighted Noah-MP's proficiency in soil moisture simulation and its strong
152 performance in Total Water Storage (TWS) simulations, while recognizing VIC's
153 capabilities in streamflow simulations.

154 Our choice of models also was informed by the varying levels of complexity
155 these two models offer in conceptualizing the effects of vegetation, soil, and seasonal
156 snowpack on the land surface energy and water balances (refer to Table 1 for more
157 details). VIC and Noah-MP employ different parameterizations for various
158 hydrological processes, such as canopy water storage, base flow, and runoff. Noah-
159 MP features four runoff physics options (see Table 1). It utilizes four soil layers, each
160 with a fixed depth. In contrast, the VIC model, with its variable infiltration capacity
161 approach (Liang et al., 1994), uses up to three soil layers per grid cell with variable
162 depths, providing flexibility in modeling soil moisture dynamics. The unique runoff
163 generation methodologies of each model are particularly pertinent for capturing the
164 diverse hydrological characteristics of the WUS.

165 The calibrated parameters we develop here for both models will provide future
166 researchers with essential tools for comprehensive hydrological analysis across the
167 WUS. Utilizing these two distinct models, each with unique strengths and methods,
168 will facilitate thorough exploration of the WUS's varied hydrological characteristics,
169 and response of the watersheds in the region to climate change, as well as
170 implementation of improved streamflow forecast methods. Our results will help to
171 facilitate a deeper understanding of hydrological processes and spatial variability
172 across the entire WUS region.

173 In our implementation of both models, we accumulated runoff over each of the
174 calibration watersheds. We chose not to implement the channel routing schemes of
175 either model since their impact on daily streamflow simulations is small given the
176 relatively small size of most of the basins. This aligns with earlier research (e.g., Li et

177 al. 2019). However, in both the case of VIC and Noah-MP, the output of our
178 simulations (runoff) could be used as input to routing models, such as those that are
179 options in the implementation of both models. We describe below the particulars of
180 the two models.

181 **2.2.1 VIC**

182 VIC is a macroscale, semi-distributed hydrologic model (described in detail by
183 Liang et al 1994) that determines land surface moisture and energy states and fluxes
184 by solving the surface water and energy balances. VIC is a research model and in its
185 various forms it has been employed to study many major river basins worldwide (e.g.
186 Adam et al 2003 & 2006; Livneh et al 2013; Schaperow et al 2021). This model
187 enjoys a broad user community — as per the citation index Web of Science, the initial
188 VIC paper has been referenced more than 2600 times, with contributing authors
189 spanning at least 56 different countries (Schaperow et al 2021). We obtained initial
190 VIC model parameters from Livneh et al 2013, who validated model discharges over
191 major CONUS river basins. The origins of the soil and land cover data are outlined in
192 Table 1. The version of the VIC model implemented here is 4.1.2, and it operates in
193 energy balance mode. We selected VIC 4.1.2 for two key reasons: First, our initial
194 parameters were based on Livneh et al. (2013), who validated model discharges over
195 major CONUS river basins using this model version. Second, in a preliminary
196 assessment of snow water equivalent (SWE) simulation skills at select SNOTEL sites
197 across the WUS, we found that VIC 4.1.2 demonstrated superior performance
198 compared to VIC 5 (see Figure S1). This finding, coupled with our research group's
199 extensive experience and proven results with VIC 4.1.2, informed our decision to use
200 this version.

201 **2.2.2 Noah-MP**

202 Noah-MP was originally designed as the land surface scheme for numerical
203 weather prediction (NWP) models like the Weather Research and Forecasting (WRF)
204 regional atmospheric model. Currently, it's being utilized for physically based,
205 spatially-distributed hydrological simulations as a component of the National Water
206 Model (NWM) (NOAA, 2016). It enhances the functionalities of the Noah LSM (as
207 per Chen et al., 1996 and Chen and Dudhia, 2001) previously used in NOAA's suite of
208 numerical weather prediction models by offering multiple options for key processes
209 that control land-atmosphere transfers of moisture and energy. These include surface
210 water infiltration, runoff, evapotranspiration, groundwater movement, and channel
211 routing (see Niu et al., 2007; 2011). The model has been widely used for forecasting
212 seasonal climate, weather, droughts, and floods not only across the continental United
213 States (CONUS) but also globally (Zheng et al., 2019). We utilized the most current
214 version (WRF-HYDRO 5.2.0)

215 **2.3 Forcing Dataset**

216 We ran both models at a 3-hour time step and at $1/16^\circ$ latitude–longitude spatial
217 resolution. The forcings were the gridded observation dataset developed by Livneh et
218 al (2013) and extended to 2018 by Su et al (2021) (hereafter referred to as L13). This
219 data set spans the period from 1915 to 2018. For the VIC model, the L13 dataset
220 provided daily values of precipitation, maximum and minimum temperatures, and
221 wind speed (additional variables used by VIC including downward solar and
222 longwave radiation, and specific humidity, are computed internally using MTCLIM
223 algorithms as described by Bohn et al. (2013)). The Noah-MP model, on the other
224 hand, necessitated additional meteorological data such as specific humidity, surface

225 pressure, and downward solar and longwave radiation, in addition to precipitation,
 226 wind speed, and air temperature. We used the MTCLIM algorithms, as detailed by
 227 Bohn et al. (2013), to calculate specific humidity and downward solar radiation. We
 228 employed the Prata (1996) algorithm to compute the downward longwave radiation.
 229 Additionally, we deduced surface air pressure by considering the grid cell elevation in
 230 conjunction with standard global pressure lapse rates. Following this, we transitioned
 231 the daily data to hourly metrics using a cubic spline to interpolate between Tmax and
 232 Tmin, and derived other variables using the methods explained by Bohn et al. (2013).
 233 Lastly, we distributed the daily precipitation evenly across three hourly intervals.

234 We used a 3-hour simulation timestep given numerical considerations with
 235 Noah-MP (which don't affect VIC, however for consistency we used a 3-hour
 236 timestep for VIC as well. Despite the fact that precipitation in particular was available
 237 daily (and hence apportioned equally to 3-hour timesteps) resolving the diurnal cycle
 238 is sometimes important in the case of snow (accumulation and ablation) processes
 239 which vary diurnally.

240 Table 1. Overview of hydrologic model components and parameter data sources.

MODEL	SNOW ACCUMULATION AND MELT	MOISTURE IN THE SOIL AND COLUMN/SURFACE RUNOFF	BASE FLOW	CANOPY STORAGE	VEGETATION DATA	SOIL DATA
VIC (V4.1.2)	Two-layer energy–mass balance model	Infiltration capacity function. Vertical movement of moisture through soil follows 1D Richards equation.	A function of the soil moisture in the third layer. Linear below a soil moisture threshold and becomes nonlinear above that threshold. [Liang et al., 1994]	Mosaic representation of different vegetation coverages at each cell.	University of Maryland 1-km Global Land Cover Classification (Hansen et al. 2000)	1-km STAT SGO database (Miller and White 1998).
NOAH-MP (WRF-HYDRO 5.2.0)	Three-layer energy–mass balance model that represents percolation	(1) TOPMODEL-based runoff scheme (2) Simple TOPMODEL-based runoff scheme with an equilibrium	Simple groundwater (hereafter SIMGM) [Niu et al., 2007]. Similar to SIMGM, but with a sealed bottom of the soil column [Niu et al.,	Semi-tile approach for computing longwave, latent heat, sensible heat and ground heat	MODIS 30-second Modified IGBP 20-category land cover product	1-km STAT SGO database (Miller and White

	, retention, and refreezing of meltwater within the snowpack.	water	table	2005]	fluxes	1998).
		(hereafter SIMTOP)				
		(3) Infiltration-excess-based surface runoff scheme		Gravitational free-drainage subsurface runoff scheme [Schaake et al., 1996]		
		(4) BATS runoff scheme, which parameterized surface runoff as a 4th power function of the top 2 m soil wetness (degree of saturation)		Gravitational free drainage [Dickinson et al.,1993]		

241 **3. Model calibration**

242 **3.1 Calibration methods**

243 The initial step in our calibration effort was to optimize the land surface
 244 parameters of the two models for the 263 WUS basins. These parameters, primarily
 245 soil properties which can exhibit a substantial degree of uncertainty, were iteratively
 246 updated via hundreds of simulations to accurately reflect streamflow conditions in
 247 each basin.

248 Our focus on calibrating soil-related parameters was based on their critical role
 249 in runoff generation. In this respect, we focused on key processes including
 250 infiltration, soil moisture storage, and groundwater recharge. The calibration of
 251 parameters that control these processes was prioritized to improve the representation
 252 of soil-water interactions, a major driver of runoff variability in the region. Given the
 253 importance of snow processes across much of the region, we conducted snow
 254 simulation verification at 20 Snow Telemetry (SNOTEL) (Natural Resources
 255 Conservation Service, 2023) sites across WUS. Our assessment (see Figure S1)
 256 indicated that the existing parameterizations for snow processes in both models
 257 reproduced observed SWE well across our study region.

258 Prior to calibration, we conducted a sensitivity analysis to identify the most

259 influential parameters for streamflow simulation in both models. We also drew on
260 insights from previous research in this respect (Mendoza et al. 2015; Hussein 2020;
261 Shi et al. 2008; Holtzman et al., 2020; Bass et al., 2023; Schaperow et al., 2023). We
262 then performed a sensitivity analysis, focusing on how variations in the most sensitive
263 parameters impacted Kling-Gupta Efficiency (KGE; Gupta et al., 2009). Based on
264 these analyses, we chose to calibrate six parameters for the VIC model and five for
265 the Noah-MP model (Table 2). For each parameter, we defined a physically viable
266 range (refer to Table 2), drawing from values utilized in prior studies (Cai et al. 2014;
267 Mendoza et al. 2015; Hussein 2020; Shi et al. 2008; Gochis et al., 2019; Holtzman et
268 al., 2020; Lahmers et al. 2021; Bass et al., 2023; Schaperow et al., 2023).

269 In recent years, the development of hydrologic model calibration has evolved
270 from manual, trial-and-error approaches to advanced automated techniques. This has
271 included a shift towards global optimization methods, notably the Shuffled Complex
272 Evolution algorithm (SCE-UA; Duan et al., 1992). Typically, SCE-UA has been
273 applied to computationally efficient models (simulation time often on the order of a
274 few minutes or less; see e.g., Franchini et al. (1998)). However, its application
275 becomes less practical with more recent distributed hydrologic models such as the
276 Noah-MP which require longer simulation times. To address these computational
277 challenges, Tolson and Shoemaker (2007) introduced the Dynamically Dimensioned
278 Search (DDS) algorithm, tailored for complex, high-dimensional problems. DDS is
279 more computationally efficient than SCE-UA, and we therefore used it for our
280 Noah-MP calibrations.

281 To assure that the parameter sets we estimated weren't dependent on the
282 optimization method, we conducted a comparison between SCE-UA and DDS for
283 calibrating VIC across 20 randomly chosen basins. We found that the DDS algorithm
284 achieved optimal calibration with fewer iterations (typically around 3000 iterations vs

285 only about 250 for DDS). The parameter sets identified were nearly identical,
 286 affirming our decision to use distinct algorithms tailored to the computational
 287 demands of each model.

288 For both models, our objective function was the KGE metric for daily
 289 streamflow. KGE is a widely used performance measure because of its advantages in
 290 orthogonally considering bias, correlation and variability (Knoben et al., 2019). KGE
 291 = 1 indicates perfect agreement between simulations and observations; KGE values
 292 greater than -0.41 indicate that a model improves upon the mean flow benchmark
 293 (Konben et al., 2019).

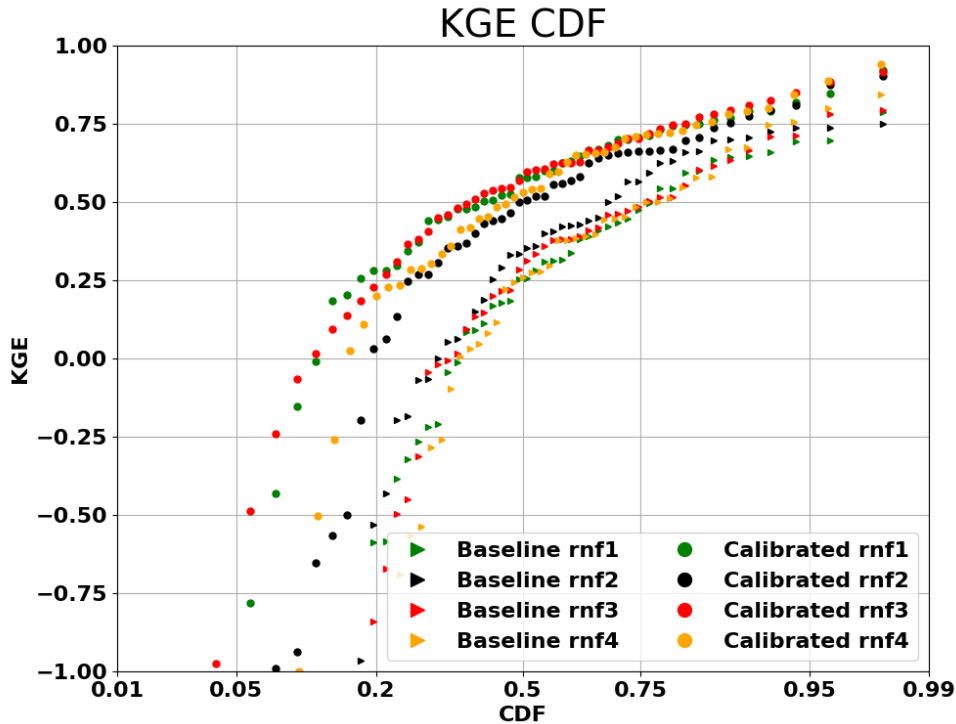
294 TABLE 2. Calibration methods, parameters and modifications to their initial
 295 default values evaluated in the calibration.

Model	VIC		Noah-MP	
Calibration Method	SCE-UA		DDS	
Iterations	3000		250	
Calibrated Parameter	Variable Infiltration Curve Parameter (INFILT)	0.001 – 0.4 (Shi et al.,2008)	Saturated Hydraulic Conductivity (Ksat)	2×10^{-9} to 0.07(Cai et al.,2014)
	Baseflow parameter (Ds)	0.001 – 1.0 (Shi et al.,2008)	Saturation soil moisture content (MAXSMC)	0.1 to 0.71 (Cai et al.,2014)
	Thickness of Soil in Layer 1 (Depth_1)	0.01 – 0.2 (Shi et al.,2008)	Pore size distribution index (Bexp)	1.12 to 22 (Cai et al.,2014; Gochis et al.,2019)
	Total thickness of soil column (Depth_total)	0.6 – 3.5 (Shi et al.,2008)	Linear scaling of “openness” of bottom drainage boundary (Slope)	0.1-1 (Lahmers et al 2021)
	Max velocity parameter of baseflow (Dsmax)	0.001 – 30 (Schaperow et al.,2023)	Parameter in surface runoff (REFKDT)	0.1-10 (Lahmers et al 2021)
	Fraction of max	0.001 – 1		

soil moisture (Shi et
where nonlinear al.,2008)
baseflow occurs
(Ws)

296 **3.2 Noah-MP parameterization**

297 As specified in Table 1, Noah-MP has four runoff and groundwater physics
298 options (rnf). Initially, we adopted the options that are incorporated in the NWM, as
299 elaborated in Gochis et al. (2020). Before we could proceed with calibrating Noah-
300 MP for all the WUS basins, it was necessary to determine suitable rnfs. To streamline
301 computational time, we initially selected 50 basins randomly from the total of 263
302 from which we created four experimental groups. Each group employed a different
303 rnf option. We applied the DDS method to these groups and compared the cumulative
304 distribution functions (CDF) of their baseline and calibrated KGEs (Figure 3). From
305 this figure, it's apparent that the KGE improved post-calibration for all four rnfs.
306 Notably, rnf3, also known as free drainage, exhibited the most substantial
307 performance enhancement after calibration. As a result, we chose to continue using
308 this option which is incorporated in the NWM. Nonetheless, it's worth noting that the
309 use of different options for different basins—a feature currently not utilized in Noah-
310 MP or WRF-Hydro—could potentially result in improved overall model performance.



311

312 Figure 3. Streamflow performance (KGE of daily streamflow simulations) of
 313 different Noah-MP runoff generation options across 50 (of 263) randomly selected
 314 basins. The performances are shown for both baseline and calibrated simulations.

315 **3.3 Calibration of gauged basins**

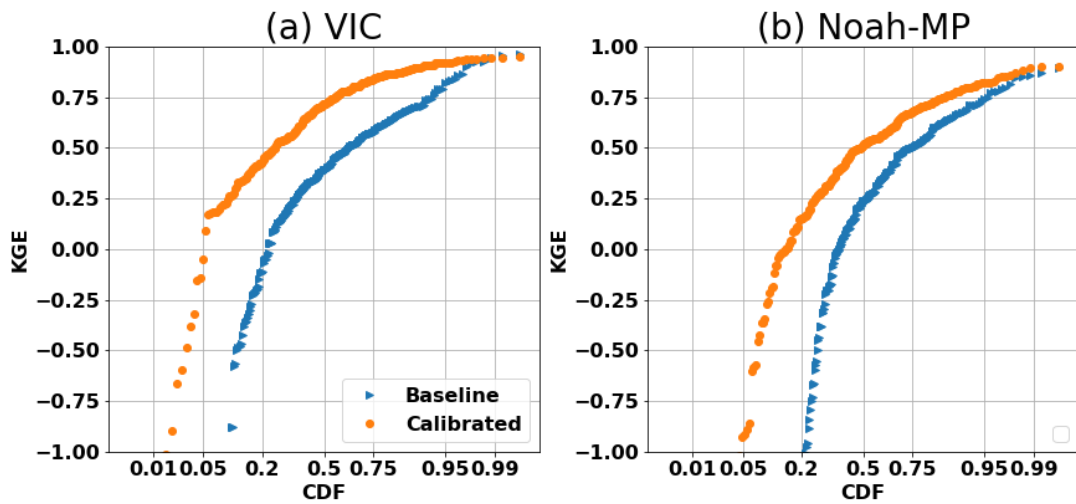
316 Following the selection of the most effective set of runoff generation options
 317 across the domain, we estimated model parameters for all 263 basins. The
 318 comparative performance of the models, before and after calibration, is shown in
 319 Figure 4. It's apparent from the figure that both Noah-MP and VIC have significantly
 320 enhanced their daily streamflow simulation skills post-calibration. After calibration,
 321 the median KGE of Noah-MP improved from 0.22 to 0.54, and the VIC's median
 322 KGE increased from 0.37 to 0.70. When contrasting the two models, we observed that
 323 VIC outperformed Noah-MP both pre- and post-calibration. One possible explanation
 324 could be that the baseline VIC parameters were taken from Livneh et al. (2013), and
 325 these parameters had already been validated and adjusted for major U.S. basins

326 (although not for our 263 basins specifically), while the Noah-MP parameters are
327 default values from NWM. Another possibility is inherent differences in the physics
328 of streamflow simulation between the two models (VIC primarily generates runoff via
329 the saturation excess mechanism), although that isn't the main focus of our research.

330 Following the calibration with data from the past 20 years, we performed a test
331 where we calibrated the streamflow using the first 10 years of data and validated with
332 the subsequent 10 years of data. This test revealed that the KGE distribution from the
333 10-year calibration is similar to that from the 20-year data. The median KGE values
334 for VIC and Noah-MP after calibration with 10 years of observations were 0.52 and
335 0.69, respectively. Correspondingly, the median KGEs during the validation period
336 were 0.50 and 0.68, respectively, which are only slightly lower. These comparisons
337 demonstrate general consistency over time in the performance of the calibrated
338 parameters.

339 To validate the robustness of our calibration methodology, we calculated
340 alternative (to KGE) performance metrics, specifically Nash-Sutcliffe Efficiency
341 (NSE) and bias. Our analyses, detailed in Figures S2&3, revealed significant
342 enhancements in model performance as measured by these metrics. The observed
343 improvements across multiple evaluation criteria affirm the efficacy of our calibration
344 process, and in particular that the performance of our procedures is not contingent
345 upon the choice of evaluation metrics.

346



347

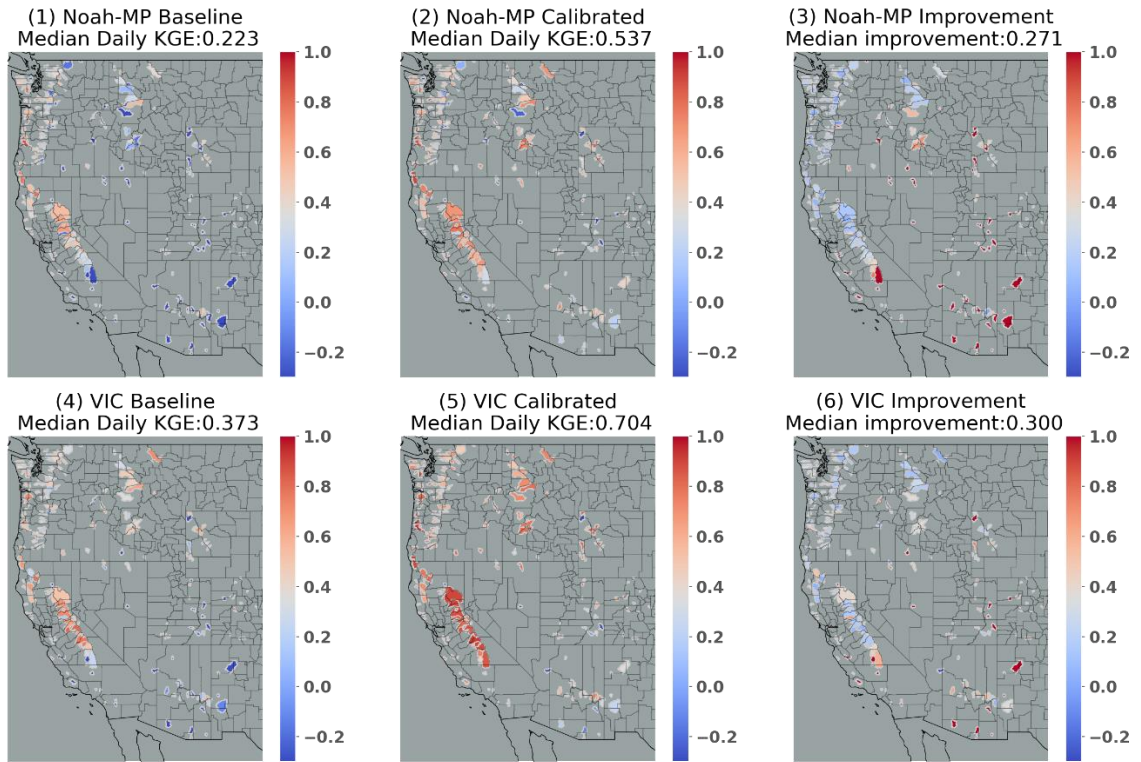
348 Figure 4. Cumulative Distribution Function (CDF) plot of the daily streamflow
 349 KGE for (a) VIC and (b) Noah-MP, comparing baseline and calibrated runs across all
 350 263 basins.

351 We examined the spatial variability of daily streamflow KGE for Noah-MP and
 352 VIC, both before and after the calibration (see Figure 5). The highest baseline KGEs
 353 are along the Pacific Coast, in central to northern CA for both models. VIC's baseline
 354 KGE generally is high in the Pacific Northwest. Post-calibration improvements
 355 occurred for both models in most areas, especially in regions where the baseline KGE
 356 was low, such as southern CA and the southeastern part of the study region. Median
 357 improvements after calibration were 0.27 for Noah-MP and 0.30 for VIC.

358 We observed that basins displaying higher KGE values typically were more
 359 humid than those with lower KGE. To further delve into the relationship between
 360 KGE and basin characteristics, we explored correlations between KGE and 21
 361 different characteristics, including drainage area, elevation, seasonal/annual average
 362 temperature and precipitation, annual maximum precipitation, and seasonal/annual
 363 runoff ratio. Of these, 12 characteristics were statistically significantly correlated with
 364 the VIC KGE, including four seasonal and annual runoff ratios; mean precipitation in
 365 winter, spring, and fall; annual maximum precipitation; and minimum elevation.

366 Figure 6 shows scatterplots of eight representative characteristics. Apart from
367 minimum elevation and mean summer temperature, all other characteristics were
368 positively correlated with KGE. Typically, spring runoff ratio, annual runoff ratio,
369 mean annual max precipitation, and mean winter precipitation exhibited the highest
370 correlations with KGE. This implies that basins with higher runoff ratios (particularly
371 in spring), higher precipitation (especially maximum precipitation), lower summer
372 temperature, and lower elevation are more likely to exhibit strong VIC performance.
373 The same applies to Noah-MP, as indicated in Figure 7, although Noah-MP showed
374 relatively weaker correlations. Correlations between mean summer temperature and
375 mean fall precipitation and Noah-MP KGE weren't statistically significant.

376 The spatial distribution of the eight characteristics is qualitatively similar with
377 the KGE spatial distribution, as shown in Figure 8. Generally, basins with higher KGE
378 have higher characteristic values when the correlation is positive, and lower
379 characteristic values when the correlation is negative. As noted above, both models
380 show good baseline performance along the Pacific Coast, and in central to northern
381 CA (Figure 5). Those areas have high runoff ratios (specifically spring and annual)
382 and high mean winter precipitation. These features generally lead to runoff physics
383 that are dominated by the saturation-excess mechanism, which is well represented by
384 both VIC and Noah-MP. VIC's baseline KGE generally is high in the inland
385 Northwest which has somewhat lower runoff ratios and (relatively) deeper
386 groundwater tables. VIC's superior performance relative to Noah-MP may also be
387 because of its variable rather than fixed soil moisture depths (as is the case for Noah-
388 MP).



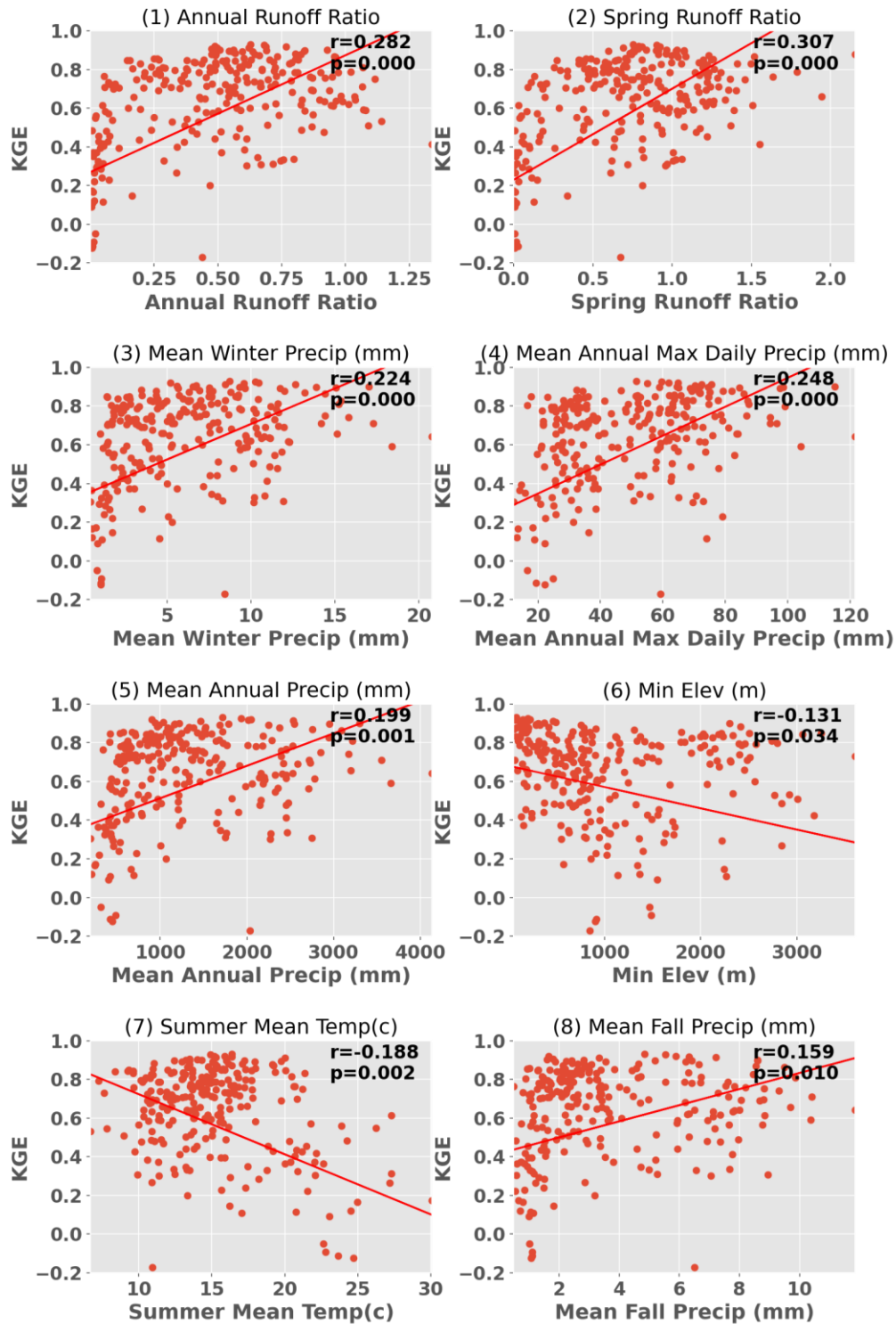
389

390 Figure 5. Spatial distribution of daily streamflow KGE for Noah-MP baseline (1);

391 calibrated Noah-MP (2); difference between calibrated and baseline Noah-MP (3);

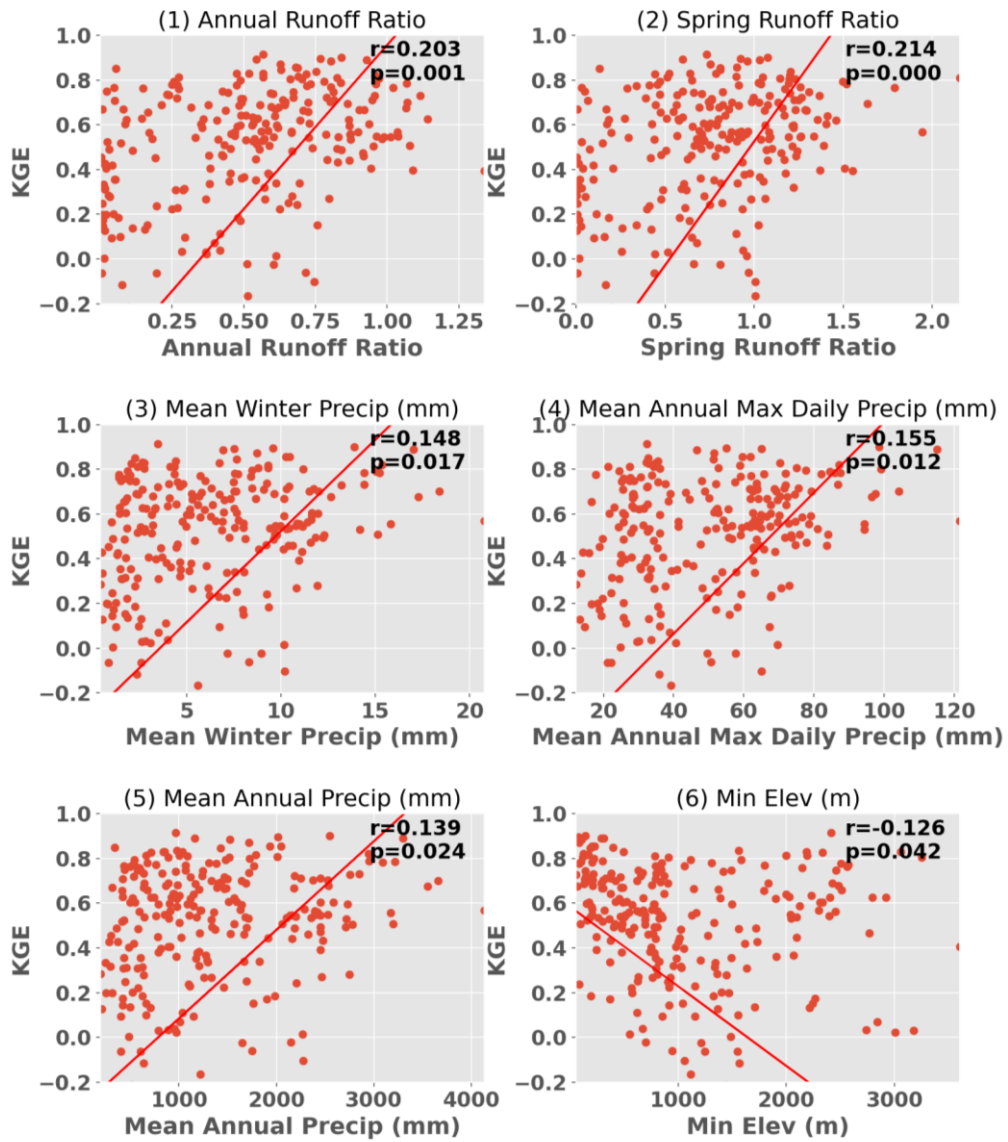
392 VIC baseline (4); calibrated VIC (5); difference between calibrated and baseline VIC

393 (6).



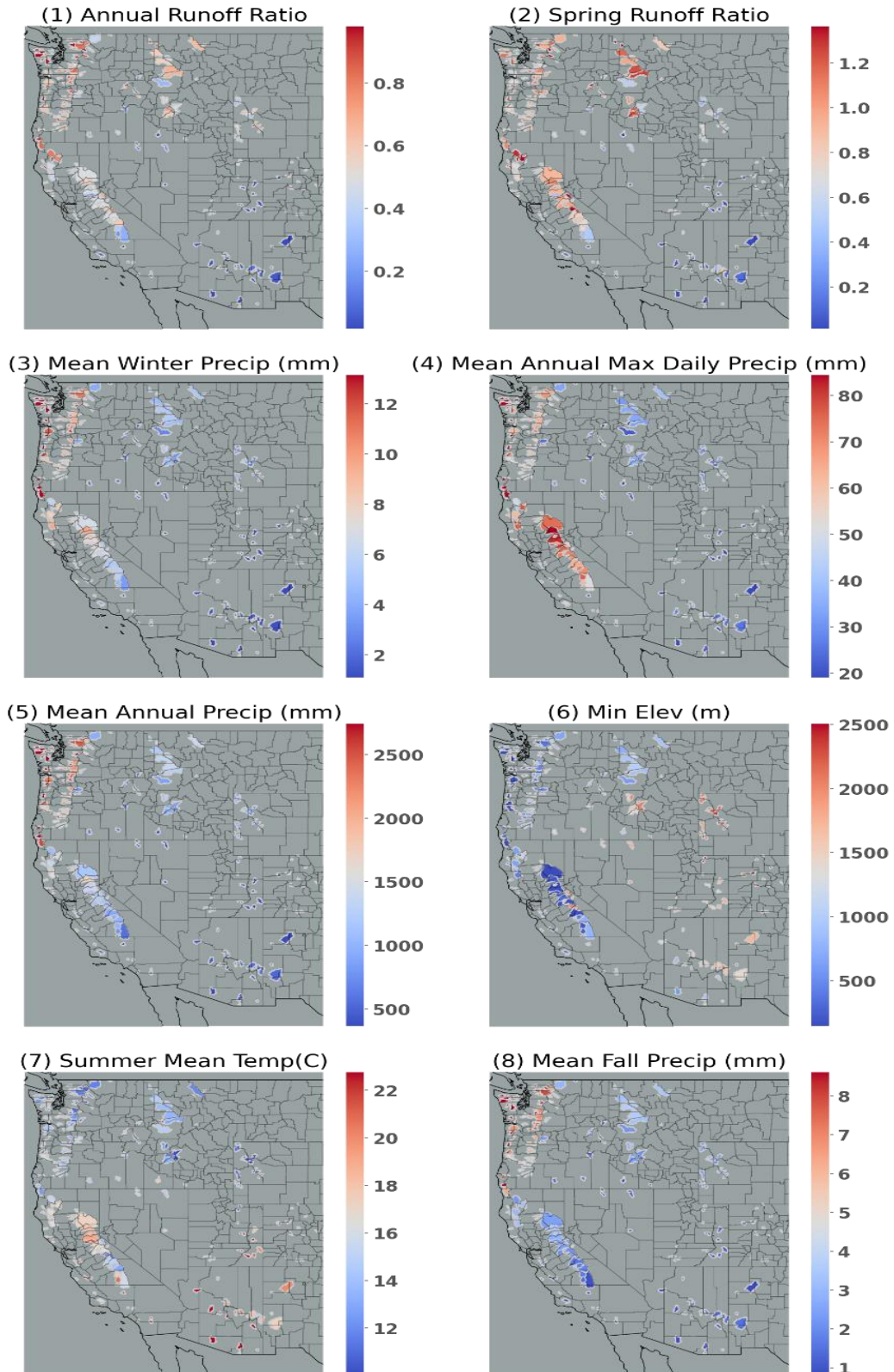
394

395 Figure 6. Scatterplots of VIC KGE in relation to significantly correlated
 396 characteristics. Each subplot indicates the corresponding Pearson correlation
 397 coefficients and the P-value.



398

399 Figure 7. Scatterplot of Noah-MP KGE in relation to significantly correlated
 400 characteristics. Each subplot indicates the corresponding Pearson correlation
 401 coefficients and the P-value.



402

403

Figure 8. Spatial distribution of characteristics that are statistically significantly

404

correlated with KGE. Note that all characteristics are significantly correlated with

405

VIC KGE whereas only (1)-(6) are significantly correlated with Noah-MP KGE.

406 **4. Regionalization**

407 To distribute parameters from the calibration basins to the entire region, we used
408 the donor-basin method as implemented in numerous previous studies (e.g., Arsenault
409 and Brissette (2014); Poissant et al. (2017); Razavi and Coulibaly (2017); Gochis et al.
410 (2019); Qi et al. (2021) and Bass et al. (2023). Following the calibration process, we
411 regionalized the parameters from gauged to ungauged basins based on a mathematical
412 assessment of the spatial and physical proximity between the gauged and ungauged
413 basins. We considered two primary methods for implementing the donor basin
414 approach. The first uses models calibrated to spatially continuous gridded runoff
415 metrics (Beck et al. 2015; Yang et al. 2019). The second approach, which we
416 ultimately adopted, calibrates models to individual gauges, then extends these
417 parameters to ungauged basins, based either on a statistical or mathematical similarity
418 measures (e.g., Arsenault and Brissette 2014; Razavi and Coulibaly 2017). Our
419 preference for the second method was guided by a key limitation of the first approach,
420 specifically it is limited to calibrating against runoff metrics, such as long-term mean
421 flow and flow percentiles, rather than streamflow time series.

422 In the donor-basin method, an ungauged basin inherits its land surface
423 parameters from the most similar gauged basin(s) (or the 'n' most similar gauged
424 basins). Here, we evaluated the similarity or proximity between gauged and ungauged
425 basins based on the similarity index SI as defined and used by Burn and Boorman
426 (1993) and Poissant et al. (2017):

$$427 \quad SI = \sum_{i=1}^k \frac{|X_i^G - X_i^U|}{\Delta X_i} \quad (1)$$

428 In Eq. 1, k stands for the total number of features considered, X_i^G represents the *i*th
429 feature of the gauged basin G, X_i^U is the *i*th feature of a specific ungauged basin, and
430 ΔX_i is the range of potential values for the *i*th feature, grounded in the data from the

431 gauged basins. This yields a unique value of SI for each gauged basin, contingent on
432 the specific ungauged basin it is compared with. Typically, gauged basins that exhibit
433 greater resemblance to the ungauged basin will have a smaller SI.

434 We assessed the donor-basin method's efficacy using a cross-validation approach,
435 where each gauged basin was treated as ungauged one at a time. The pseudo-
436 ungauged basin inherits its hydrological parameters from its three most similar
437 gauged basins, determined by SI. The parameters inherited are a weighted average
438 from the three donor basins. After testing one to five donor basins, we found that
439 using three donors yielded the best results. Thus, every basin inherits parameters from
440 the three most similar gauged basins in each simulation, offering a concise evaluation
441 of the donor-basin method's regionalization performance.

442 We used 18 basin-specific features in the donor basin method, detailed in Table
443 S1, calculated based on the forcings and parameters used in the study. For feature
444 selection in the donor-basin method, we adopted an iterative approach, explained in
445 detail in the following paragraph. Only basins with a KGE exceeding 0.3 were
446 considered, following previous studies suggesting that inclusion of poorly performing
447 basins can lower regionalization performance. We found that a KGE threshold of 0.3
448 resulted in a median performance improvement of 0.08 larger than did a KGE
449 threshold of 0, hence it was chosen. After screening, 223 basins were utilized in VIC
450 regionalization and 194 in Noah-MP regionalization. We note that the parameters used
451 for calibration and the features used to determine the similarity index in the
452 regionalization process are different. The physics that control the key hydrological
453 processes of the two models are different, so we explored their best regionalization
454 features separately.

455 To determine the most effective regionalization features from the 18 basin
456 characteristics listed in Table S1, we employed a systematic iterative approach. The

457 first iteration includes 18 simulations, each of which incorporates one of the 18
458 features. The feature that yielded the greatest increase in the median KGE across all
459 basins, based on leave-one-out cross validation, was then retained. In the second
460 iteration, we conducted 17 simulations, each combining the retained feature from the
461 first iteration with one of the remaining 17 features. This process was repeated
462 iteratively, reducing the number of features considered in each subsequent round, until
463 the addition of new features no longer resulted in an appreciable increase in median
464 KGE. The sequence of features shown in Figure 9 (also shown in Table S1) indicated
465 the importance of the features. This iterative approach ensured that each feature's
466 individual and combined contribution to model performance was thoroughly assessed.
467 It allowed us to identify a subset of features that, when used together, optimally
468 improved model accuracy. We recognize the potential existence of inter-feature
469 correlations that may exert a discernible influence on their collective efficacy when
470 utilized in combination.

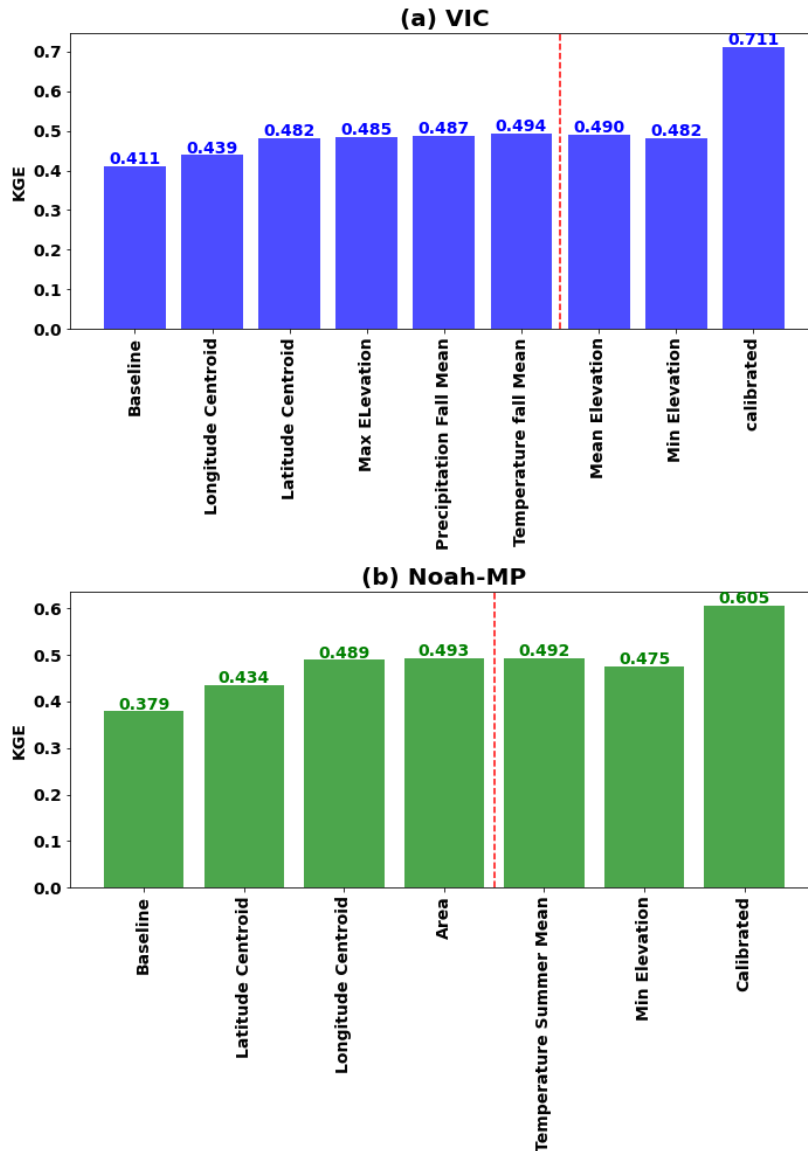
471 This procedure resulted in five features generated the best regionalization
472 performance for VIC (longitude centroid, latitude centroid, maximum elevation, fall
473 mean precipitation, and fall mean temperature). Three features were found to be best
474 for Noah-MP (latitude centroid, longitude centroid, and drainage area) (see Figure 9).
475 Among them, latitude and longitude are the common features that contribute the most
476 to regionalization when using the similarity index method. This suggests that
477 geographical similarities are the most important factor in parameter information
478 transfer from gauged to ungauged basins.

479 Upon evaluating the performance of baseline, calibrated, and regionalized
480 simulations, the respective median daily KGEs for the VIC model were found to be
481 0.41, 0.71, and 0.49. For the Noah-MP, these values were 0.38, 0.60, and 0.49 (refer
482 to Figures 9 & S4). These metrics are for basins that have a calibrated KGE greater

483 than 0.3 only, resulting in higher median KGEs than for all 263 basins (See Figure 4).
484 The KGE distribution also improved overall. It's noteworthy that the regionalization
485 improvement relative to baseline is higher for Noah-MP than for VIC. While VIC's
486 baseline and calibrated KGE skill distribution outperforms Noah-MP's, the differences
487 between regionalized skills of Noah-MP and VIC are decreasing. We will explore
488 more on this in the following section.

489 After optimizing the features and specific design of the donor-basin method,
490 parameters were regionalized to 4816 ungauged USGS Hydrologic Unit Code (HUC)
491 -10 basins across the WUS. HUCs are delineated and quality controlled by USGS
492 using high-resolution DEMs. For each of the 4816 HUC-10 basins, we calculated a
493 similarity index with the calibrated basins using the selected features. The three most
494 similar basins were identified as donor basins, and their weighted average parameters
495 were then adopted by the target HUC-10 basin. The final hydrologic parameters for
496 both VIC and Noah-MP for all WUS HUC-10 basins are shown in Figures S5&6.
497 The baseline HUC-10 parameters are shown in Figures S7&8.

498 Comparison of Figures S5-6 to Figures S7-8 makes it clear that the baseline
499 model parameters lack accuracy, and exhibit significant spatial uniformity where large
500 geographical regions share identical parameter values. For example, parameters such
501 as *Ds* and *Soil_Depth1* in VIC show this uniformity. Furthermore, certain parameters,
502 such as *SLOPE* and *REFKDT* in Noah-MP, remain invariant across all spatial
503 domains, and don't reflect real-world conditions. Regionalization, improved the
504 parameters, leading to increased accuracy and strengthening of region-specific
505 characteristics.



506

507 Figure 9. Best regionalization features for (a) VIC and (b) Noah-MP. The final
 508 regionalization to ungauged basins of the WUS incorporated all features up to the
 509 point marked by the red line since the addition of further features doesn't improve
 510 KGE.

511 **5. Evaluation of calibration and regionalization skills**

512 Our primary calibration objective was to enhance the accuracy of daily
 513 streamflow simulations. However, to ensure the versatility of our parameter sets for
 514 research related to both floods and dry conditions, we also evaluated the models'
 515 capabilities in reproducing high and low streamflow. To understand the capabilities of

516 the two models in reconstructing high and low streamflow, we assessed their
517 performance across baseline, calibrated, and regionalized settings.

518 (a) Evaluation of high flow performance

519 We used the peaks-over-threshold (POT) method (Lang et al. 1999) to identify
520 extreme streamflow events as in Su et al (2023) and Cao et al. (2019, 2020). We first
521 applied the event independence criteria from USWRC (1982) to daily streamflow data
522 to identify independent events. We set thresholds at each basin that resulted in 3
523 extreme events per year on average (denoted as POT3). After selecting the flood
524 events over the study period based on the observation, we sorted the floods based on
525 the return period and then calculated the KGE of baseline, calibrated and regionalized
526 floods. Figure S9 displays the associated CDF plots. The median KGE for baseline
527 floods in Noah-MP was 0.14, which rose to 0.37 post-calibration, and receded to 0.22
528 after regionalization. For VIC, the flood KGE started at 0.11, increased to 0.41 after
529 calibration, and declined to 0.20 post-regionalization. As anticipated, these numbers
530 are lower than (all) daily streamflow skill due to our calibration target being daily
531 streamflow. Still, flood competencies experienced considerable enhancement,
532 surpassing the Noah-MP KGE benchmark of -0.41 found by Knoben et al. (2019).

533 (b) Evaluation of low flow performance

534 (c) To assess low flow performance, we utilized the 7q10 metric. This
535 hydrological statistic, commonly adopted in water resources management
536 and environmental engineering, is the lowest 7-day average flow that occurs
537 (on average) once every 10 years (EPA,2018). Scatterplots of 7q10 (Figure
538 S10) showed high correlation between our model's simulated low flows and
539 the observed data. Post-calibration, this alignment intensified. The VIC
540 model tended to underestimate the low flows. After calibration, the median
541 bias improved from -23.6% to -9.9%, and with regionalization, it was -11.7%.

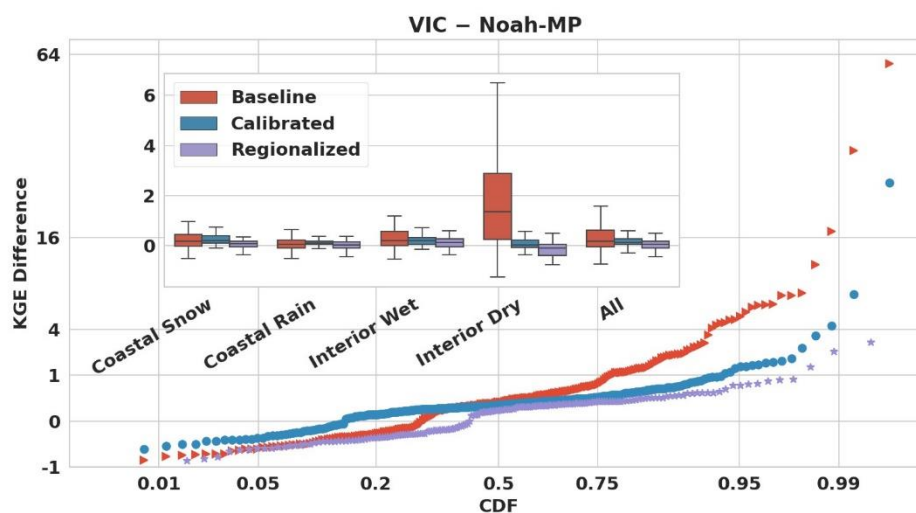
542 In contrast, Noah-MP began with an 11.20% overestimation in the baseline,
543 improved to 0.61% post-calibration, and was -9.5% after regionalization. The
544 outcomes underline the proficiency of both models for low flow prediction,
545 exhibiting enhanced competencies post-calibration and commendable
546 performance after regionalization. Comparison of VIC and Noah-MP
547 simulation skill

548 In Section 4, we demonstrated that while VIC's baseline and calibrated daily
549 streamflow KGE skill distribution was better than Noah-MP's, the disparity was
550 reduced following regionalization. We further explored the skill differences between
551 the two models for baseline, calibrated, and regionalized parameters for different
552 hydroclimatic conditions. Figure 10 shows the CDF of the daily streamflow KGE
553 differences between VIC and Noah-MP across the study basins. The skill gap between
554 VIC and Noah-MP generally narrows from baseline through calibrated to regionalized
555 runs, although VIC outperforms Noah-MP in most of the basins for all three runs.

556 We further divided the study region into four different categories following
557 Huang et al (2021): coastal snow dominated basins, coastal rain dominated, interior
558 wet, and interior dry. In the baseline runs (Figure 10 and 11.1), VIC generally
559 outperforms Noah-MP with a median KGE difference of 0.168, particularly in interior
560 dry basins, and in some interior wet and coastal basins. Following calibration (Figure
561 10 and 11.2), the median KGE difference decreases to 0.126. VIC has superior
562 performance in most of the basins, especially interior wet and coastal basins. In
563 interior dry basins (mostly in the southeastern part of our domain), VIC's performance
564 is similar to or worse than Noah-MP's. This discrepancy is attributable to more
565 pronounced improvements in VIC after calibration in coastal and northern WUS,
566 while Noah-MP shows greater improvements in the southeastern WUS (mostly dry
567 interior). Post-regionalization (Figure 10 and 11.3), the KGE differences further

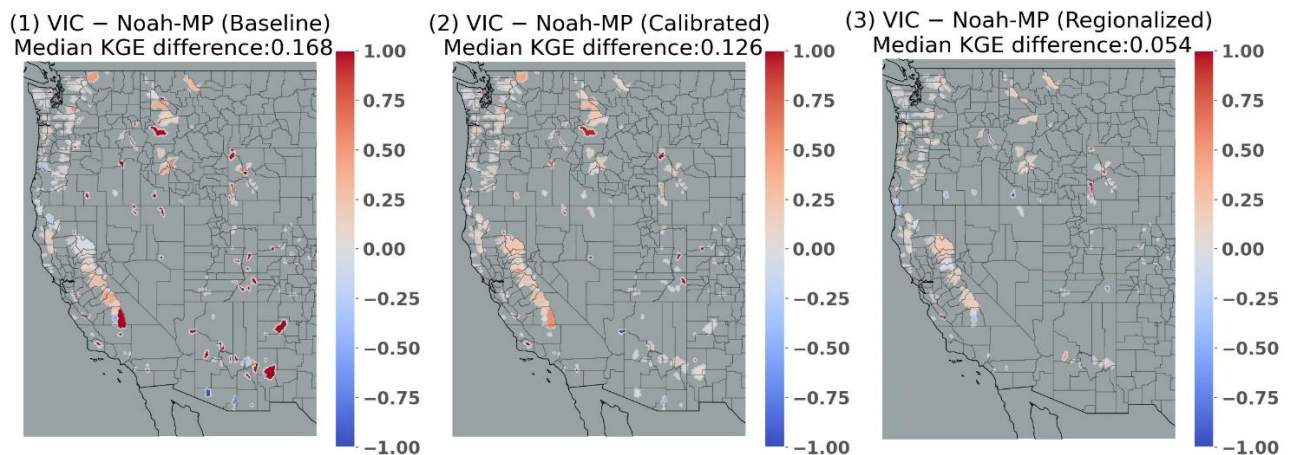
568 narrow to a median of 0.054, with VIC still outperforming Noah-MP in most coastal
 569 and interior wet basins. Nonetheless, VIC is inferior in a few interior dry basins
 570 scattered across WUS, where both models exhibit relatively low skill. This is also
 571 shown in Figure S11 CDFs which indicate that VIC's performance varies notably
 572 across the spectrum: it falls below Noah-MP at the lower end of the skill distribution.
 573 Conversely, VIC KGEs exceed those of Noah-MP in areas where its skill is strongest.
 574 Across all basins collectively, VIC outperforms Noah-MP post regionalization as
 575 evidenced by higher VIC median skill (Figure 10 inset).

576 We also evaluated the performance of the two models after regionalization in
 577 simulating annual average flows, flood flows (POT3), and low flows (measured as
 578 7q10). The results (see Figures S12 and S13) show that VIC outperforms Noah-MP in
 579 simulating annual mean streamflow (Figure S12) and (in most cases) floods (Figure
 580 S13). Conversely, Noah-MP generally performs better in simulating low flows (Figure
 581 S10).



582
 583 Figure 10. Cumulative distribution function (CDF) plot of the daily streamflow KGE
 584 differences between VIC and Noah-MP in the study basins for baseline, calibrated and
 585 regionalized runs. The inset figure shows boxplots of KGE differences for four

586 different categories: coastal snow dominated basins (54 basins), coastal rain
587 dominated basins (103 basins), interior wet basins (53 basins), and interior dry basins
588 (53 basins). We also show all basins collectively (263 total) for reference purposes.

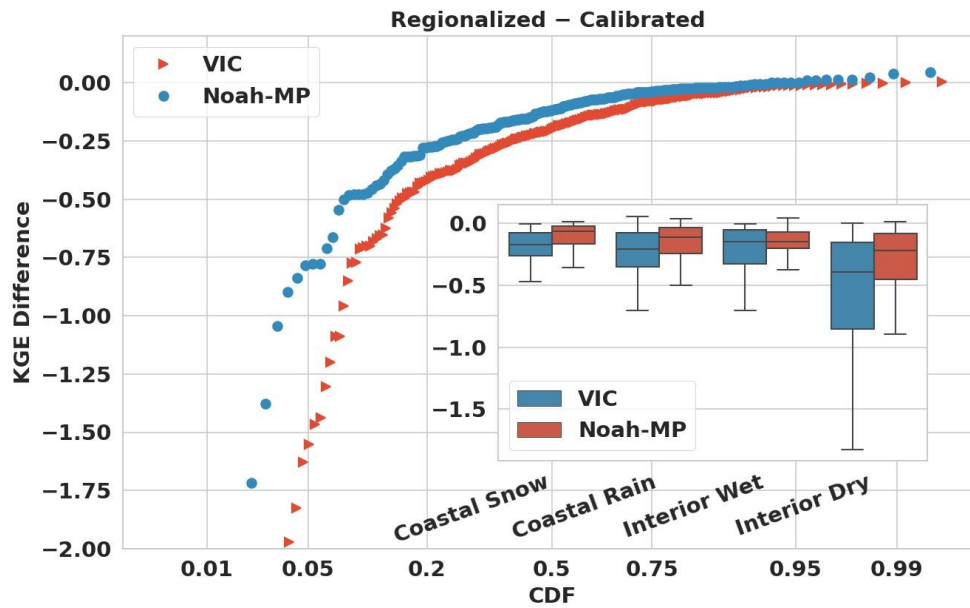


589
590 Figure 11. Map of the daily streamflow KGE differences between VIC and
591 Noah-MP in the study basins for (1) baseline, (2) calibrated and (3) regionalized runs.

592 (d) Comparison of post-regionalization and post-calibration performance

593 We further analyzed the performance differences between the regionalized and
594 calibrated runs for each model. As depicted in Figure 12, both VIC and Noah-MP
595 have declining skill for post-regionalization relative to post-calibration runs, with VIC
596 demonstrating a more pronounced decrease, reflected in a median KGE difference of -
597 0.199, compared to -0.117 for Noah-MP. For both models, coastal basins and interior
598 wet basins tend to have smaller skill decreases from post-calibration to post-
599 regionalization; and interior dry basins have the largest skill decreases. VIC has
600 greater decreases than Noah-MP in most basins. The most significant drops in
601 performance generally occur in basins where baseline skills are low, yet post-
602 calibration skills are relatively high.

603



604

605 Figure 12. CDF of differences of daily streamflow skill between regionalized and
 606 calibrated for VIC and Noah-MP. The inset figure summarizes KGE difference
 607 distributions for the same four categories as the inset in Figure 10.

608 **6. Discussion**

609 We summarize our key accomplishments in calibrating the two hydrological
 610 models, examine our approach to choosing calibration objective functions and metrics,
 611 and we consider lessons learned in model regionalization.

612 (a) Improved parameter sets

613 We generated calibrated parameter sets for the VIC and Noah-MP hydrological
 614 models at $1/16^\circ$ latitude-longitude scale across WUS. These calibrated parameter sets
 615 are intended to facilitate the use of the two models for climate change and water
 616 investigations across the region, among other applications. Our focus on calibrating
 617 daily streamflow aligns with common practice in hydrology, providing a
 618 comprehensive representation of catchment hydrology dynamics which should
 619 enhance future understanding of hydrological phenomena and their spatial variations
 620 across the region.

621 (b) Selection of calibration objective function

622 We used objective functions based on streamflow observations. We chose this
623 approach due to its applicability elsewhere, given the widespread accessibility of
624 streamflow observations as compared to alternative metrics such as soil moisture or
625 evapotranspiration (Demaria et al., 2007; Gao et al., 2018; Troy et al., 2008; Yadav et
626 al., 2007). While we acknowledge the potential of remote sensing products like
627 MODIS, SMAP, SMOS, ESA, and ALEXI to improve calibration efforts, especially
628 for variables like actual evapotranspiration (AET) and soil moisture (SM), we were
629 limited by the scarcity of observations for these variables. Future studies could,
630 nonetheless, leverage from the methods we've employed to incorporate additional
631 variables into the objective functions we used.

632 (c) Selection of calibration metric

633 We used the KGE metric applied to daily streamflow, which we chose for its
634 ability to address bias, correlation, and variability simultaneously (Knoben et al.,
635 2019). We also evaluated NSE and BIAS metrics, and found substantial
636 improvements in both models' performance after calibration when these metrics were
637 used in place of KGE (See Figures S2-3). Our assessment of high and low flow
638 reconstruction in Section 5 further validated our generated parameter sets. While we
639 used a single objective function due to data and computing constraints, incorporating
640 multiple objective functions is feasible in principle.

641 (d) Regionalization possibilities

642 We calibrated model parameters directly for individual basins, considering their
643 unique hydrological features, and then transferred these calibrated parameters to
644 similar basins based on similarity assessments. Alternative parameter transfer
645 strategies could be used within the same framework we employed (e.g., pedo-transfer
646 functions, e.g. Imhoff et al., 2020) or multiscale parameter regionalization (e.g.

647 Schwappe et al.,2022). We do note that our regionalization approach facilitates the
648 transfer of calibrated parameters to comparable regions, which could be explored in
649 future research.

650 **7. Conclusions**

651 Our intent was to develop a regional parameter estimation strategy for the VIC
652 and Noah-MP land surface schemes, and to apply it across the WUS region at the
653 HUC-10 catchment scale. We've described what we believe is a robust framework
654 that can be applied in future hydrological and climate change studies across the WUS,
655 and is applicable to other regions as well. Our key findings and conclusions are:

- 656 a) Our catchment scale calibration of the two models to 263 sites across WUS
657 resulted in major improvements in the performance of both models relative to
658 a priori parameters, but performance improvement was greatest for Noah-
659 MP – although this may be in part because VIC a priori parameters benefitted
660 from prior calibration and hence resulted in better baseline performance than
661 did a priori Noah-MP.
- 662 b) Both models performed best in more humid basins, mainly in the Pacific
663 Northwest and central to northern CA where runoff ratios are high. This is
664 consistent with previous results (e.g. Bass et al.,2023).
- 665 c) Post-calibration regional model performance improved for both models in
666 most areas, especially where the baseline KGE was low, such as southern CA
667 and the southeastern part of the study region.
- 668 d) VIC performance across all calibration basins was mostly better than for
669 Noah-MP. However, Noah-MP performance benefitted more from
670 regionalization than did VIC, and ultimately post-regionalization VIC
671 performance was only slightly superior to that of Noah-MP. When
672 partitioned into hydroclimatic categories, VIC outperforms Noah-MP in all

673 but interior dry basins following regionalization, where Noah-MP is better.
674 e) Post-regionalization, both VIC and Noah-MP performance declines in
675 comparison with the calibrated run, with declines more pronounced for VIC.
676 The performance degradation is greatest in interior dry basins for both
677 models.
678 f) VIC outperforms Noah-MP in simulating annual mean streamflow and flood
679 simulations in most cases. Conversely, Noah-MP performs better for low
680 flows. These results should provide guidance for selecting the most
681 appropriate model depending on the hydrological condition being analyzed.

682

683 **Data Availability statement**

684 The Livneh (2013) forcings are available at
685 <http://livnehpublicstorage.colorado.edu:81/Livneh.2013.CONUS.Dataset/>. The
686 extended forcings used in this study are available at [ftp://livnehpublicstorage.](ftp://livnehpublicstorage.colorado.edu/public/sulu)
687 [colorado.edu/public/sulu](ftp://livnehpublicstorage.colorado.edu/public/sulu). The results are available online at
688 <https://figshare.com/s/66fe8305bff516e80f6f> .

689

690

691

692 **Author contribution**

693 LS and DL conceptualized the study. LS generated the dataset and analysis with
694 support of DL, MP and BB. LS drafted the manuscript with support of DL.

695

696 **Competing interests.** The contact author has declared that none of the authors has
697 any competing interests.

698

699 **References**

- 700 Adam, J.C. and Lettenmaier, D.P.: Adjustment of global gridded precipitation for
701 systematic bias, *J. Geophys. Res.*, 108(D9), 1-14, doi:10.1029/2002JD002499,
702 2003.
- 703 Adam, J.C., Clark, E.A. , Lettenmaier, D.P. and Wood, E.F.: Correction of Global
704 Precipitation Products for Orographic Effects, *J. Clim.*, 19(1), 15-38, doi:
705 10.1175/JCLI3604.1, 2006.
- 706 Anghileri, D., Voisin, N., Castelletti, A., Pianosi, F. , Nijssen, B. and Lettenmaier, D.P.:
707 Value of Long-Term Streamflow Forecasts to Reservoir Operations for Water
708 Supply in Snow-Dominated River Catchments. *Water Resources Research* 52:
709 4209–25, 2016.
- 710 Arsenault, R., and Brissette, F. P.: Continuous streamflow prediction in ungauged
711 basins: The effects of equifinality and parameter set selection on uncertainty in
712 regionalization approaches. *Water Resour. Res.*, 50, 6135–6153, [https://doi.org/](https://doi.org/10.1002/2013WR014898)
713 10.1002/2013WR014898, 2014.
- 714 Bass, B., Rahimi, S., Goldenson, N., Hall, A., Norris, J. and Lebow, Z.J.: Achieving
715 Realistic Runoff in the Western United States with a Land Surface Model Forced
716 by Dynamically Downscaled Meteorology. *Journal of Hydrometeorology*, 24(2),
717 269-283, 2023.
- 718 Beck, H. E., Roo, A. de and van Dijk, A. I. J. M.: Global maps of streamflow
719 characteristics based on observations from several thousand catchments. *J.*
720 *Hydrometeor.*, 16, 1478–1501, <https://doi.org/10.1175/JHM-D-14-0155.1>, 2015.
- 721 Bennett, A. R., Hamman, J. J. and Nijssen, B.: MetSim: A Python package for
722 estimation and disaggregation of meteorological data. *J. Open Source Software*,
723 5, 2042, <https://doi.org/10.21105/joss.02042>, 2020.
- 724 Beven, K.: Changing ideas in hydrology-the case of physically-based models. *Journal*

725 of Hydrology, 105(1-2), 157–172. [https://doi.](https://doi.org/10.1016/0022-1694(89)90101-7)
726 [org/10.1016/0022-1694\(89\)90101-7](https://doi.org/10.1016/0022-1694(89)90101-7), 1989.

727 Bohn, T. J., Livneh, B., Oyler, J. W., Running, S. W., Nijssen, B. and Lettenmaier, D.
728 P.: Global evaluation of MTCLIM and related algorithms for forcing of
729 ecological and hydrological models. *Agric. For. Meteor.*, 176, 38–49,
730 <https://doi.org/10.1016/j.agrformet.2013.03.003>, 2013.

731 Burn, D. H., and Boorman, D. B.: Estimation of hydrological parameters at ungauged
732 catchments. *J. Hydrol.*, 143,429454, [https://doi.org/10.1016/0022-](https://doi.org/10.1016/0022-1694(93)90203-L)
733 [1694\(93\)90203-L](https://doi.org/10.1016/0022-1694(93)90203-L), 1993.

734 Cai, X., Yang, Z.-L. , David, C. H., Niu, G.-Y. and Rodell, M.: Hydrological
735 evaluation of the Noah-MP land surface model for the Mississippi River Basin. *J.*
736 *Geophys. Res. Atmos.*, 119, 23–38, <https://doi.org/10.1002/2013JD020792>, 2014.

737 California Department of Water Resources: California data exchange center: Daily
738 full natural flow for December 2022. California Department of Water Resources,
739 accessed 1 October 2021, [https://cdec.water.ca.gov/reportapp/javareports?name=](https://cdec.water.ca.gov/reportapp/javareports?name=FNF)
740 [FNF](https://cdec.water.ca.gov/reportapp/javareports?name=FNF), 2021.

741 Cao, Q., Mehran, A. , Ralph, F. M. and Lettenmaier, D. P.: The role of hydrological
742 initial conditions on atmospheric river floods in the Russian River basin. *J.*
743 *Hydrometeor.*, 20, 16671686, <https://doi.org/10.1175/JHM-D-19-0030.1>, 2019.

744 Cao, Q., Gershunov, A., Shulgina, T., Ralph, F. M. , Sun, N. and Lettenmaier, D. P.:
745 Floods due to atmospheric rivers along the U.S. West Coast: The role of
746 antecedent soil moisture in a warming climate. *J. Hydrometeor.*, 21, 1827–1845,
747 [https:// doi.org/10.1175/JHM-D-19-0242.1](https://doi.org/10.1175/JHM-D-19-0242.1), 2020.

748 Castiglioni, S., Lombardi, L., Toth, E. , Castellarin, A. and Montanari, A.: Calibration
749 of rainfall-runoff models in ungauged basins: A regional maximum likelihood
750 approach. *Advances in Water Resources*, 33(10), 1235–1242.

751 <https://doi.org/10.1016/j.advwatres.2010.04.009>, 2010.

752 Chen, F., and Dudhia, J.: Coupling an advanced land surface–hydrology model with
753 the Penn State–NCAR MM5 modeling system. Part I: Model implementation
754 and sensitivity. *Mon. Wea. Rev.*, 129, 569–585, [https://doi.org/10.1175/1520-0493\(2001\)129<0569:CAALSH>2.0.CO;2](https://doi.org/10.1175/1520-0493(2001)129<0569:CAALSH>2.0.CO;2), 2001.

756 Chen, F., and Coauthors: Modeling of land-surface evaporation by four schemes and
757 comparison with FIFE observations. *J. Geophys. Res.*, 101, 7251–7268,
758 <https://doi.org/10.1029/95JD02165>, 1996.

759 Cosby, B.J., Hornberger, G.M., Clapp, R.B. and Ginn, T.: A statistical exploration of
760 the relationships of soil moisture characteristics to the physical properties of soils.
761 *Water resources research*, 20(6), 682–690, 1984.

762 Demaria, E. M., Nijssen, B., & Wagener, T.: Monte Carlo sensitivity analysis of land
763 surface parameters using the Variable Infiltration Capacity model. *Journal of*
764 *Geophysical Research*, 112, D11113. <https://doi.org/10.1029/2006JD007534>,
765 2007.

766 Dembélé M, Hrachowitz M, Savenije H.H, Mariéthoz G, Schaepli B.: Improving the
767 predictive skill of a distributed hydrological model by calibration on spatial
768 patterns with multiple satellite data sets. *Water resources research*,
769 Jan;56(1):e2019WR026085, <https://doi.org/10.1029/2019WR026085>, 2020

770 Demirel, M. C., Mai, J., Mendiguren, G., Koch, J., Samaniego, L., and Stisen, S.:
771 Combining satellite data and appropriate objective functions for improved spatial
772 pattern performance of a distributed hydrologic model, *Hydrol. Earth Syst. Sci.*,
773 22, 1299–1315, <https://doi.org/10.5194/hess-22-1299-2018>, 2018.

774 Dickinson, R. E., Henderson-Sellers, A. & Kennedy, P. J.: Biosphere–Atmosphere
775 Transfer Scheme (BATS) version 1e as coupled to the NCAR Community
776 Climate Model. NCAR Tech. Note TN383+STR, NCAR, 1993.

777 Duan, Q., Sorooshian, S. and Gupta, V. : Effective and efficient global optimization
778 for conceptual rainfall-runoff models. *Water Resour. Res.*, 28, 1015–1031,
779 [https://doi.org/ 10.1029/91WR02985](https://doi.org/10.1029/91WR02985), 1992.

780 Environmental Protection Agency (EPA) Office of Water: Low Flow Statistics Tools:
781 A How-To Handbook for NPDES Permit Writers. EPA-833-B-18-001, 2018.

782 Falcone, J.: GAGES-II: Geospatial attributes of gages for evaluating streamflow. U.S.
783 Geological Survey, accessed 1 April 2021,
784 [https://water.usgs.gov/GIS/metadata/usgswrd/XML/ gagesII_Sept2011.xml](https://water.usgs.gov/GIS/metadata/usgswrd/XML/gagesII_Sept2011.xml), 2011.

785 Fisher, R.A. and Koven, C.D.: Perspectives on the future of land surface models and
786 the challenges of representing complex terrestrial systems. *Journal of Advances*
787 *in Modeling Earth Systems*, 12(4), p.e2018MS001453, 2020.

788 Franchini, M., Galeati, G. and Berra S.: Global optimization techniques for the
789 calibration of conceptual rainfall-runoff models, *Hydrol. Sci. J.*, 43, 443 – 458,
790 1998.

791 Gao, H., Birkel, C., Hrachowitz, M., Tetzlaff, D., Soulsby, C., & Savenije, H. H.
792 (2018). A simple topography-driven, calibration-free runoff generation model.
793 *Hydrology and earth system sciences discussions.*,1–42.
794 <https://doi.org/10.5194/hess-2018-141>

795 Gochis, D. and Coauthors: Overview of National Water Model Calibration: General
796 strategy and optimization. National Center for Atmospheric Research, accessed 1
797 January 2023, 30 pp.,
798 https://ral.ucar.edu/sites/default/files/public/9_RafieeiNasab_CalibOverview_CU
799 [AHSI_Fall019_0.pdf](https://ral.ucar.edu/sites/default/files/public/9_RafieeiNasab_CalibOverview_CU), 2019.

800 Gong, W., Duan, Q., Li, J., Wang, C., Di, Z., Dai, Y., et al.: Multi-objective parameter
801 optimization of common land model using adaptive surrogate modeling.
802 *Hydrology and Earth System Sciences*, 19(5), 2409–2425.

803 <https://doi.org/10.5194/hess-19-2409-2015>, 2015.

804 Gou, J., Miao, C., Duan, Q., Tang, Q., Di, Z., Liao, W., Wu, J. and Zhou, R.:

805 Sensitivity analysis-based automatic parameter calibration of the VIC model for

806 streamflow simulations over China. *Water Resources Research*, 56(1),

807 e2019WR025968, 2020.

808 Gupta, H. V., et al.: Decomposition of the mean squared error and NSE performance

809 criteria: Implications for improving hydrological modelling. *Journal of*

810 *Hydrology*, 377, 80-91,2009.

811 Holtzman, N.M., Pavelsky, T.M., Cohen, J.S., Wrzesien, M.L. and Herman, J.D.:

812 Tailoring WRF and Noah-MP to improve process representation of Sierra

813 Nevada runoff: Diagnostic evaluation and applications. *Journal of Advances in*

814 *Modeling Earth Systems*, 12(3), p.e2019MS001832, 2020.

815 Huang, H., Fischella, M., Liu, Y. , Ban, Z. , Fayne, J. , Li, D. , Cavanaugh, K. and

816 Lettenmaier, D.P.: Changes in mechanisms and characteristics of Western U.S.

817 floods over the last sixty years. *Geophysical Research Letters*, 49, DOI:

818 10.1029/2021GL097022, 2021

819 Hussein, A.: Process-based calibration of WRF-hydro model in unregulated

820 mountainous basin in Central Arizona. M.S. thesis, Ira A. Fulton Schools of

821 Engineering, Arizona State University, 110 pp.,

822 [https://keep.lib.asu.edu/_flysystem/fedora/](https://keep.lib.asu.edu/_flysystem/fedora/c7/224690/Hussein_asu_0010N_19985.pdf)

823 [c7/224690/Hussein_asu_0010N_19985.pdf](https://keep.lib.asu.edu/_flysystem/fedora/c7/224690/Hussein_asu_0010N_19985.pdf), 2020.

824 Imhoff, R.O., Van Verseveld, W.J., Van Osnabrugge, B. and Weerts, A.H.: Scaling

825 point-scale (pedo) transfer functions to seamless large-domain parameter

826 estimates for high-resolution distributed hydrologic modeling: An example for

827 the Rhine River. *Water Resources Research*, 56(4), p.e2019WR026807,2020.

828 Fisher, R. A. and Koven, C. D. : Perspectives on the Future of Land Surface Models

829 and the Challenges of Representing Complex Terrestrial Systems. *Journal of*
830 *Advances in Modeling Earth Systems*, 12(4),
831 <https://doi.org/10.1029/2018MS001453>, 2020. Kimball, J. S., Running, S. W.
832 and Nemani, R. R.: An improved method for estimating surface humidity from
833 daily minimum temperature. *Agric. For. Meteor.*, 85, 87–98, [https://](https://doi.org/10.1016/S0168-1923(96)02366-0)
834 [doi.org/10.1016/S0168-1923\(96\)02366-0](https://doi.org/10.1016/S0168-1923(96)02366-0), 1997.

835 Lahmers, T.M., et al.: Evaluation of NOAA national water model parameter
836 calibration in semiarid environments prone to channel infiltration. *Journal of*
837 *Hydrometeorology*, 22(11), 2939-2969, 2021.

838 Li, D., Lettenmaier, D. P., Margulis, S. A. and Andreadis, K.: The role of rain-on-
839 snow in flooding over the conterminous United States. *Water Resour. Res.*, 55,
840 8492–8513, <https://doi.org/10.1029/2019WR024950>, 2019.

841 Liang, X., Lettenmaier, D. P., Wood, E. F. and Burges S. J.: A simple hydrologically
842 based model of land surface water and energy fluxes for general circulation
843 models. *J. Geophys. Res.*, 99(D7), 14415–14428, doi:10.1029/94JD00483, 1994.

844 Livneh B, Rosenberg, E.A., Lin, C., Nijssen, B., Mishra, V., Andreadis, K., Maurer,
845 E.P. and Lettenmaier, D.P.: A long-term hydrologically based data set of land
846 surface fluxes and states for the conterminous United States: Updates and
847 extensions, *Journal of Climate*, doi:10.1175/JCLI-D-12-00508.1, 2013.

848 Maidment, D.R.: Conceptual Framework for the National Flood Interoperability
849 Experiment. *Journal of the American Water Resources Association* 53: 245–57,
850 2017.

851 Mascaro, G., Hussein, A., Dugger, A. and Gochis, D.J.: Process-based calibration of
852 WRF-Hydro in a mountainous basin in southwestern US. *Journal of the*
853 *American Water Resources Association*, 59(1), 49-70, 2023.

854 Mendoza, P.A., Clark, M.P., Mizukami, N., Newman, A.J., Barlage, M., Gutmann,

855 E.D., Rasmussen, R.M., Rajagopalan, B., Brekke, L.D. and Arnold, J.R.: Effects
856 of hydrologic model choice and calibration on the portrayal of climate change
857 impacts. *Journal of Hydrometeorology*, 16(2), 762-780, 2015.

858 Miller, D.A. and White, R.A.: A conterminous United States multilayer soil
859 characteristics dataset for regional climate and hydrology modeling. *Earth
860 interactions*, 2(2), pp.1-26, 1998.

861 Mizukami, N., Clark, M. P., Newman, A. J., Wood, A. W., Gutmann, E. D., Nijssen,
862 B. , Rakovec, O. and Samaniego, L. :Towards seamless large-domain parameter
863 estimation for hydrologic models. *Water Resour. Res.*, 53, 8020–8040, [https://
864 doi.org/10.1002/2017WR020401](https://doi.org/10.1002/2017WR020401), 2017.

865 Naeini, M.R., Analui, B., Gupta, H.V., Duan, Q. and Sorooshian, S.. Three decades of
866 the Shuffled Complex Evolution (SCE-UA) optimization algorithm: Review and
867 applications. *Scientia Iranica*, 26(4), 2015-2031, 2019.

868 Natural Resources Conservation Service: SNOTEL (Snow Telemetry) Data. USDA.
869 <https://www.nrcs.usda.gov/wps/portal/wcc/home/>, 2023.

870 Niu, G.-Y., Yang, Z.-L. , Dickinson, R. E. , Gulden, L. E. and Su, H.: Development of
871 a simple groundwater model for use in climate models and evaluation with
872 gravity recovery and climate experiment data. *J. Geophys. Res.*, 112, D07103,
873 <https://doi.org/10.1029/2006JD007522>, 2007.

874 Niu, G. Y., Yang, Z. L., Dickinson, R. E., & Gulden, L. E.: A simple
875 TOPMODEL-based runoff parameterization (SIMTOP) for use in global climate
876 models. *Journal of Geophysical Research: Atmospheres*, 110(D21), 2005.

877 Niu, G.-Y., and Coauthors: The community Noah land surface model with
878 multiparameterization options (Noah-MP): 1. Model description and evaluation
879 with local-scale measurements. *J. Geophys. Res.*, 116, D12109,
880 <https://doi.org/10.1029/2010JD015139>, 2011.

881 NOAA (National Oceanic and Atmospheric Administration): National Water Model:
882 Improving NOAA's Water Prediction Services, 2016.

883 Oubeidillah, A. A., Kao, S.-C., Ashfaq, M. , Naz, B. S. and Tootle, G.: A large-scale,
884 high-resolution hydrological model parameter data set for climate change impact
885 assessment for the conterminous US. Hydrology and Earth System Sciences,
886 18(1), 67–84. [https://doi.org/ 10.5194/hess-18-67-2014](https://doi.org/10.5194/hess-18-67-2014), 2014.

887 Prata, A.J.: A new long-wave formula for estimating downward clear-sky radiation at
888 the surface. Quarterly Journal of the Royal Meteorological Society, 122(533),
889 1127-1151, 1996.

890 Poissant, D., Arsenault, A. and Brissette, F. : Impact of parameter set dimensionality
891 and calibration procedures on streamflow prediction at ungauged catchments. J.
892 Hydrol. Reg. Stud., 12,220–237, <https://doi.org/10.1016/j.ejrh.2017.05.005>, 2017.

893 Qi, W.Y., Chen, J. , Li, L. , Xu, C.-Y. , Xiang, Y.-h. , Zhang, S.-B. and Wang, H.-M.:
894 Impact of the number of donor catchments and the efficiency threshold on
895 regionalization performance of hydrological models. J. Hydrol., 601, 126680,
896 <https://doi.org/10.1016/j.jhydrol.2021.126680>, 2021.

897 Raff, D., Brekke, L. , Werner, K. , Wood, A. and White. K.: Short-Term Water
898 Management Decisions: User Needs for Improved Climate, Weather, and
899 Hydrologic Information. U.S. Bureau of Reclamation.
900 <https://www.usbr.gov/research/st/roadmaps/WaterSupply.pdf>, 2013.

901 Razavi, T., and Coulibaly, P.: An evaluation of regionalization and watershed
902 classification schemes for continuous daily streamflow prediction in ungauged
903 watersheds. Can. Water Resour. J., 42,2–20,
904 <https://doi.org/10.1080/07011784.2016.1184590>, 2017.

905 Rajsekhar, D., Singh, V.P. and Mishra, A.K., 2015. Hydrologic drought atlas for Texas.
906 Journal of Hydrologic Engineering, 20(7), p.05014023.

907 Schaake, J. C., Koren, V. I., Duan, Q.-Y., Mitchell, K., & Chen, F.: Simple water
908 balance model for estimating runoff at different spatial and temporal scales.
909 Journal of Geophysical Research, 101(D3), 7461–7475.
910 <https://doi.org/10.1029/95JD02892>, 1996.

911 Schaperow J.R, Li, D., Margulis, S.A., Lettenmaier D.P. :A near-global, high
912 resolution land surface parameter dataset for the variable infiltration capacity
913 model. Scientific Data. Aug 11;8(1):216, 2021.

914 Schweppe, R., Thober, S., Müller, S., Kelbling, M., Kumar, R., Attinger, S., and
915 Samaniego, L.: MPR 1.0: a stand-alone multiscale parameter regionalization tool
916 for improved parameter estimation of land surface models, Geosci. Model Dev.,
917 15, 859–882, <https://doi.org/10.5194/gmd-15-859-2022>, 2022.

918 Sharma, P. and Machiwal, D.: Streamflow forecasting: overview of advances in data-
919 driven techniques. Advances in Streamflow Forecasting,1-50.
920 <https://doi.org/10.1016/B978-0-12-820673-7.00013-5>, 2021

921 Shi, X., Wood, A.W. and Lettenmaier, D.P. : How essential is hydrologic model
922 calibration to seasonal streamflow forecasting? Journal of Hydrometeorology,
923 9(6), 1350-1363, 2008.

924 Sofokleous, I., Bruggeman, A., Camera, C. and Eliades, M.: Grid-based calibration of
925 the WRF-Hydro with Noah-MP model with improved groundwater and
926 transpiration process equations. Journal of Hydrology, 617, 128991 , 2023

927 Su, L., Cao, Q. , Xiao, M., Mocko, D. M., Barlage, M. , Li, D. , Peters-Lidard, C. D.
928 and Lettenmaier, D. P.: Drought variability over the conterminous United States
929 for the past century. J. Hydrometeor., 22, 1153–1168,
930 <https://doi.org/10.1175/JHM-D-20-0158.1>, 2021.

931 Su, L., Cao, Q. , Shukla, S., Pan, M. and Lettenmaier, D.P.: Evaluation of Subseasonal
932 Drought Forecast Skill over the Coastal Western United States. Journal of

933 Hydrometeorology, 24(4), 709-726, 2023.

934 Tangdamrongsub, N.: Comparative Analysis of Global Terrestrial Water Storage
935 Simulations: Assessing CABLE, Noah-MP, PCR-GLOBWB, and GLDAS
936 Performances during the GRACE and GRACE-FO Era. *Water*, 15(13), p.2456,
937 2023.

938 Thornton, P. E., and Running, S. W.: An improved algorithm for estimating incident
939 daily solar radiation from measurements of temperature, humidity, and
940 precipitation. *Agric. For. Meteor.*, 93, 211–228, [https://doi.org/10.1016/S0168-](https://doi.org/10.1016/S0168-1923(98)00126-9)
941 [1923\(98\)00126-9](https://doi.org/10.1016/S0168-1923(98)00126-9), 1999.

942 Tolson, B. A., and Shoemaker, C. A.: Dynamically dimensioned search algorithm for
943 computationally efficient watershed model calibration. *Water Resour. Res.*, 43,
944 W01413, <https://doi.org/10.1029/2005WR004723>, 2007.

945 Troy, T. J., Wood, E. F. and Sheffield, J.: An efficient calibration method for
946 continental-scale land surface modeling. *Water Resources Research*, 44, W09411.
947 <https://doi.org/10.1029/2007WR006513>, 2008

948 USWRC: Guidelines for determining flood flow frequency. Bulletin 17B of the
949 Hydrology Subcommittee, 183 pp., [https://](https://water.usgs.gov/osw/bulletin17b/dl_flow.pdf)
950 water.usgs.gov/osw/bulletin17b/dl_flow.pdf, 1982.

951 Yang, Y., Pan, M., Beck, H.E. , Fisher, C.K., Beighley, R.E. , Kao, S.C. , Hong, Y. and
952 Wood, E.F.: In quest of calibration density and consistency in hydrologic
953 modeling: Distributed parameter calibration against streamflow characteristics.
954 *Water Resources Research*, 55(9), 7784-7803, 2019.

955 Yadav, M., Wagener, T., & Gupta, H. (2007). Regionalization of constraints on
956 expected watershed response behavior for improved predictions in ungauged
957 basins. *Advances in Water Resources*, 30(8), 1756–1774.
958 <https://doi.org/10.1016/j.advwatres.2007.01.005>

959 Zheng, H., Yang, Z.-L. , Lin, P. , Wei, J. , Wu, W.-Y., Li, L. , Zhao, L. and Wang, S.:

960 On the sensitivity of the precipitation partitioning into evapotranspiration and

961 runoff in land surface parameterizations. *Water Resour. Res.*, 55, 95–111,

962 <https://doi.org/10.1029/2017WR022236>, 2019.

963 Zink M, Mai J, Cuntz M, Samaniego L. Conditioning a hydrologic model using

964 patterns of remotely sensed land surface temperature. *Water Resources Research*.

965 2018 Apr;54(4):2976-98.

966